JOURNAL OF GEOPHYSICAL RESEARCH, VOL. 101, NO. D3, PAGES 7431–7448, MARCH 20, 1996

Linkage of scaling and thermodynamic parameters of rainfall: Results from midlatitude mesoscale convective systems

S. Perica[1] and E. Foufoula-Georgiou

Department of Civil Engineering, Saint Anthony Falls Laboratory, University of Minnesota
Minneapolis

Abstract. In this paper we explore the possibility of establishing predictive relationships between statistical characteristics of rainfall at the mesoscale (approximately 10^2 to 10^4 km^2) and representative meteorological parameters of the storm environment. To increase the usefulness of these relationships and, in particular, to explore their use in subgrid-scale rainfall parameterization, special attention is given to statistical characteristics of rainfall that are scale invariant, i.e., are constant at least within a significant range of scales. The main contributions of this paper are the following: (1) we establish the presence of statistical (simple) scaling in "standardized rainfall fluctuations" (derived from rainfall intensities via an orthogonal wavelet transform and normalization by local means) and (2) we establish empirical connections between statistical and physical storm characteristics by quantifying relations between the scaling parameters and kinematic and thermodynamic indices of the prestorm environment. The data used for this analysis are rainfall events and corresponding soundings observed during the PRE-STORM experiment (May and June 1985) over Oklahoma and Kansas. The developed relationships are applicable to midlatitude mesoscale convective systems, which are the major rainfall producers over most of the Global Energy and Water Cycle Experiment (GEWEX) Continental International Project (GCIP) region, and are envisioned to play a key role in disaggregating rainfall (predicted by mesoscale numerical models) to subgrid scales for runoff prediction and other hydrologic applications.

1. Introduction

A problem of continuous interest in rainfall research is that of relating statistical parameterizations to physical properties of rainfall for the purpose of gaining better understanding of the physics responsible for the observed rainfall structure and providing the ability to attach physical meaning and interpretation to statistical parameters of rain.

Initial attempts to address this problem were based on introducing continuous time-space conceptual models of rain, e.g., the temporal Neyman-Scott models [e.g., *Rodriguez-Iturbe et al.,* 1984] and the WGR spatiotemporal model [*Waymire et al.,* 1984]. The basic idea behind these conceptual models was the desire to mimic the observed clustering in time and hierarchical organization in space of rainfall fields [e.g., *Austin and Houze,* 1972]. These models were heavily overparameterized (e.g., the WGR model has 14 parameters) and were obviously plagued with problems of parameter estimation from limited discrete rainfall data. The parameters of these models, although estimated from statistical properties of rainfall, were intended to have physical meaning simply by model construction, e.g., rate of arrival of storms, velocity of rain cells, etc. However, the inability to directly validate this hypothesis as well as questions of lack of robustness of parameter estimates from rainfall observations at different scales (e.g., see *Foufoula-Georgiou and Guttorp* [1987] for an example in temporal rainfall models) contributed to abandoning this route of trying to relate physical and statistical characteristics of rain.

Over the past decade, evidence for the presence of scaling in spatial rainfall has been presented by several researchers. It is beyond the scope of this article to review the literature on rainfall scaling models, so the reader is referred to *Foufoula-Georgiou and Krajewski* [1995] for a review of pertinent articles during the period of 1991 to 1994. Brief summaries of developments prior to 1991 can be found in the articles by *Tessier et al.*

[1]Now at NOAA/NWS/Hydrologic Research Laboratory, Silver Spring, Maryland.

Paper number 95JD02372.
0148-0227/96/95JD-02372$05.00

[1993] and *Gupta and Waymire* [1993]. The presence of scaling (simple or multiscaling) implies that small- and large-scale statistical properties of the field are related to each other by a scale-changing operator involving only the scale ratio (absence of characteristic scale). Scaling models of rain provide attractive parsimonious representations over a wide range of scales and because of their concise parameterization offer a unique opportunity for a fresh look into the problem of relating physical and statistical characteristics of rain. The research described in this paper focuses on this issue and seeks to study empirical relationships between scale invariant statistical parameters of rainfall and physical parameters describing the storm environment.

The approach we follow to study scale invariant relationships of spatial rainfall builds on the work of *Kumar and Foufoula-Georgiou* [1993a]. In that work, spatial rainfall was decomposed in large-scale averages and "multiscale rainfall fluctuations" using orthogonal wavelet transforms. These multiscale rainfall fluctuations (wavelet coefficients) were found to exhibit scaling over a significant range of scales for two storm events (a heavy intensity squall line storm and a moderate intensity winter storm) over Norman, Oklahoma [*Kumar and Foufoula-Georgiou,* 1993b]. The scaling parameters were found to depend on the type of the storm system suggesting that they might be usefully related to physical quantities describing the storm environment. This observation provided the impetus for the present work, where we further explore this hypothesis and seek to establish quantitative relationships. The data used for our analysis are radar rainfall and rawinsonde observations from several storms over Oklahoma and Kansas during the PRE-STORM experiment in May and June 1985.

Establishing predictive relationships between statistical and physical characteristics of rainfall is not only of scientific interest but also has important practical applications. One such application is to subgrid-scale parameterization of spatial rainfall (see for example, discussion in the concluding remarks of *Kumar and Foufoula-Georgiou* [1993b]). This application is implicit in the present research and is used in the next section to motivate the significance of multiscale rainfall fluctuations, since it is these "derived" rainfall quantities and not rainfall intensities themselves that are used in our developments. Namely, this work sets forth and extensively tests two main hypotheses: (1) that "standardized rainfall fluctuations" (to be defined in section 2) exhibit simple scaling over the mesoscale and (2) that the scaling parameters of "standardized rainfall fluctuations" relate to kinematic and thermodynamic descriptors of the storm environment.

This paper is structured as follows: In section 2 we define "rainfall fluctuations," first at an intuitive level and then at a more rigorous level. Section 3 presents the data used to test the two hypotheses and establishes the scaling of "standardized rainfall fluctuations" for midlatitude mesoscale systems. In section 4, predictive relationships between the scaling parameters and the convective available potential energy (CAPE), which is a descriptor of convective instability, are established for midlatitude mesoscale convective systems. Finally, some concluding remarks are made in section 5.

2. Definition of Multiscale Rainfall Fluctuations

2.1. Intuitive Explanation and Significance

The precipitation output of numerical models (mesoscale weather prediction models or global circulation models) is usually interpreted as an average rainfall over the grid cell of the model. Since rainfall exhibits considerable heterogeneity, this average value is necessarily much lower compared to precipitation values over much smaller scales, e.g., over grid cells of 4×4 km (the resolution of the radar measurements). For runoff production over the numerical model grid cells or for subgrid-scale interpretation of climate model results it is necessary to redistribute the single large-scale average rainfall value over smaller subgrid cells, i.e., recreate or simulate the small-scale rainfall variability given its large-scale average. Before one is ready to provide solutions to this problem (that is, go from large to small scales), it is imperative to extensively study and understand the rainfall variability as a function of scale, i.e., study how the statistical properties of rainfall change as one averages over larger and larger scales (i.e., going from small to larger scales).

Consider for simplicity a one-dimensional process or function $\{x_1, x_2, ..., x_N\}$, which can be thought of as representing the sampling of a continuous process $X(t)$ at the original scale or at relative scale $\lambda = 1$ (scale index $m = 0; \lambda = 2^m$). What happens when we start aggregating this process to larger and larger scales? Obviously, by taking averages to go to the next larger scale, some information is thrown away. Only if this information is kept would one be able to reconstruct the small-scale original process from the process at the next larger scale. To fix ideas, let us consider only eight values of the aforementioned process, i.e., $\{x_1, x_2, ..., x_8\}$ at scale $\lambda = 1$. At the next level of aggregation we average two consecutive nonoverlapping values of the process and we end up with four average values instead of eight original values (relative scale $\lambda = 2, m = 1$) (see Figure 1). In doing this averaging, we threw away some information and we can never get back the original values $\{x_1, ..., x_8\}$ from the average values $\{(x_1 + x_2)/2, ..., (x_7 + x_8)/2\}$ unless some additional information, for example, the differences of consecutive nonoverlapping values at the original scale $\{(x_1 - x_2)/2, ..., (x_7 - x_8)/2\}$, is also kept. Going to larger and larger scales (until in this example we exhaust our data), we can see from Figure 1 that if one was given the large-scale average value at relative scale $\lambda = 8$ ($\overline{X}_3$) and the differences at that scale

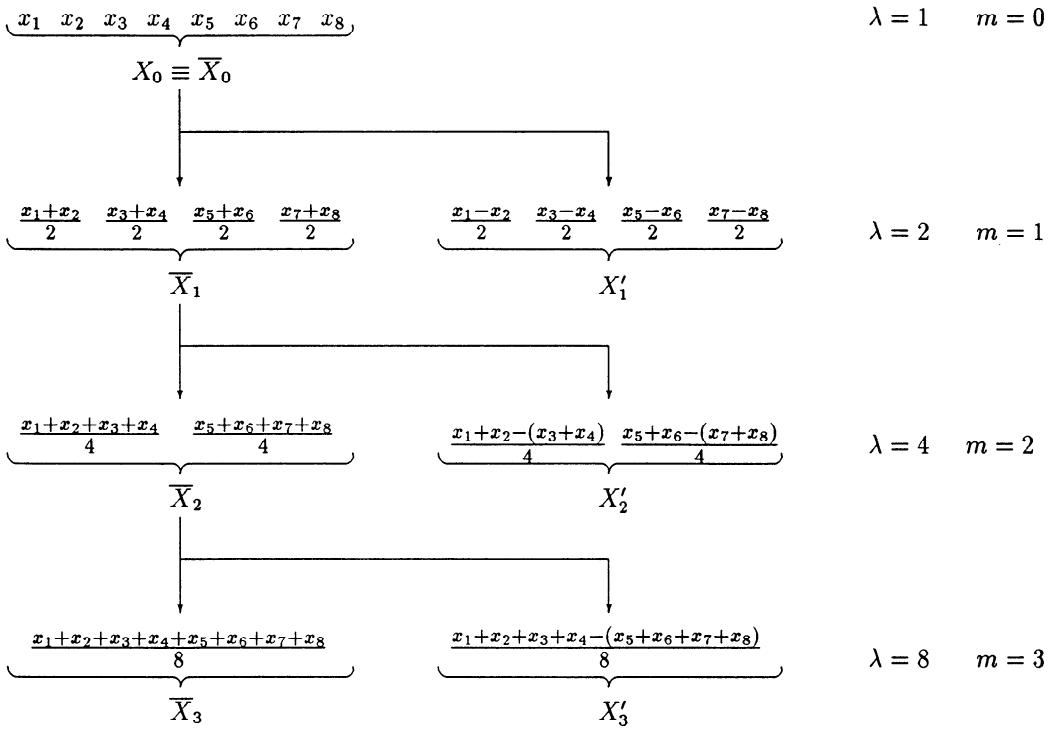

Figure 1. Schematic showing the concept of fluctuations using the Haar wavelet for a discrete one-dimensional process. Relative scales λ and scale indices m ($\lambda = 2^m$) are also indicated in the figure.

and two previous scales (i.e., X'_3, X'_2, and X'_1), then one could reconstruct the original process X_0 and the process at any intermediate scale. Note that in a stochastic framework, one would only need a statistical description of these differences at all relevant scales (i.e., stochastic models for X'_1, X'_2, and X'_3) and not their exact values. For any such application a parsimonious statistical description of these differences at all scales (which can be achieved only if scale invariant relationships are present) would be highly desirable (but not necessary).

The physical interpretation of these differences at a particular scale is that they represent "local fluctuations" around means at the next larger scale. From the above discussion it is seen that these "local fluctuations" at several scales of interest (called hereafter "multiscale local fluctuations") are important quantities to characterize in a natural process, especially if reconstruction of the small-scale variability from large-scale averages is needed. There are several added advantages in working with these multiscale local fluctuations. First, they are stationary even if the original process has a steplike trend (first-order differences remove a constant level effect; higher-order differences can be constructed to remove higher-order trends in the original signal). Second, they are local, with a locality region that depends on the scale at which the process is viewed. Third, they represent the minimal incremental information one would need to move from one scale to the next smaller scale and thus are very relevant quantities for subgrid-scale parameterization. It is for these reasons that in this paper we concentrate on statistical characterization of multiscale rainfall fluctuations and their linkage with environmental parameters of rain.

In the one-dimensional example presented earlier, the rainfall process at scale λ was obtained by applying a box filter ϕ_λ of width λ and height $1/\lambda$ (Figure 2a) to the original signal. The filter was moved along the signal to cover all observations in a nonoverlapping fashion. Corresponding differences at scale λ were obtained by applying another filter ψ_λ to the original process (Figure 2b) that has the same width as the averaging filter, but its integral is zero. This filter was also moved over nonoverlapping positions at each scale. The procedure was repeated at all scales λ of interest. Note that (1) these filters have a finite support which varies with scale, and filters at all scales are obtained by dilation of the unique filters ϕ and ψ at the original scale; (2) the averaging filters ϕ_λ and the differencing filters ψ_λ are complementary to each other, because whatever information is lost by applying ϕ_λ on the process is captured by applying ψ_λ on it; and (3) there is a consistency across scales since one will arrive at the same decomposition regardless of the scale at which filtering was initiated. In this example (Figure 2) the choice of the averaging and differencing filters result in the Haar wavelet transform of a process. Generalization of these filters to smoother filters, e.g., Gaussian, or filters in two or higher dimensions is possible and can be

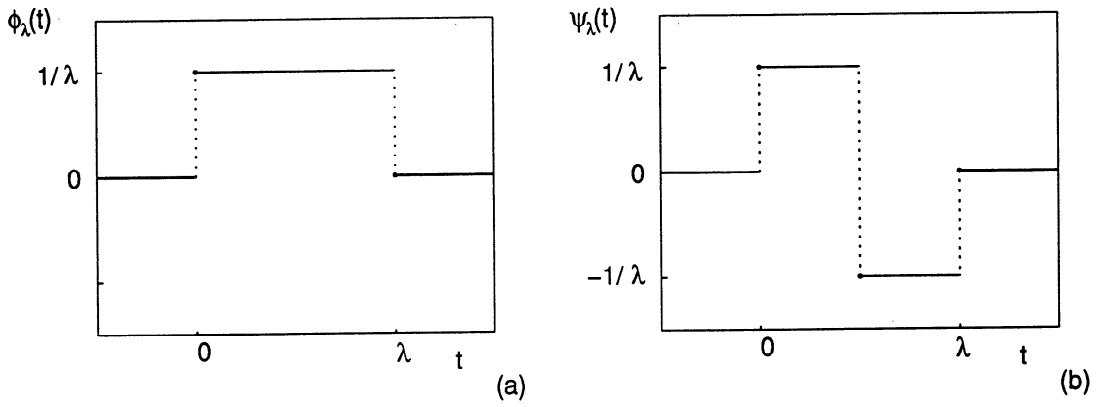

Figure 2. (a) Scaling function $\phi_\lambda(t)$ and (b) wavelet $\psi_\lambda(t)$ for a Haar wavelet transform.

efficiently and rigorously achieved within a multiresolution orthogonal wavelet decomposition framework. In fact, the simple filter of Figure 2b is the so-called Haar wavelet in one dimension.

Such a general multiscale analysis framework for spatial rainfall was presented by *Kumar and Foufoula-Georgiou* [1993a]. Below, we briefly define the two-dimensional multiscale rainfall fluctuations within the wavelet analysis framework as these fluctuations play an important role in our further developments. The reader is referred to *Kumar and Foufoula-Georgiou* [1993a] for more details.

2.2. Definition Via Wavelets

Having in mind the example decomposition of Figure 1 let us extend the discussion to a continuous stochastic process $X(t)$. We obtain versions of the process $X(t)$ at larger scales λ by applying two filters to the original process: the filter $\phi_{\lambda,u}(t)$ for "averaging" and the filter $\psi_{\lambda,u}(t)$ for "differencing." These filters can be obtained by dilation and translation of a single function $\phi(t)$ and $\psi(t)$, respectively, as

$$\phi_{\lambda,u}(t) \equiv \frac{1}{\lambda}\phi\left(\frac{t-u}{\lambda}\right) \tag{1}$$

$$\psi_{\lambda,u}(t) \equiv \frac{1}{\lambda}\psi\left(\frac{t-u}{\lambda}\right) \tag{2}$$

where λ is a scale and u is a location parameter. The function $\phi(t)$ is called the scaling function and satisfies $\int_{-\infty}^{\infty}\phi(t)\,dt = 1$; $\psi(t)$ is called the wavelet function and satisfies $\int_{-\infty}^{\infty}\psi(t)\,dt = 0$. The weights $1/\lambda$ are chosen such that $\int\phi_{\lambda,u}(t)\,dt$ is preserved at all scales. "Averages" or "generalized averages" of $X(t)$ at a particular scale λ are obtained by an integral transform of $X(t)$ with $\phi_{\lambda,u}(t)$; that is,

$$\overline{X}_\lambda(u) = \int_{-\infty}^{\infty} X(t)\phi_{\lambda,u}(t)\,dt \tag{3}$$

and "differences" or "generalized differences" are obtained by another integral transform of $X(t)$ with the wavelet function $\psi_{\lambda,u}(t)$; that is,

$$X'_\lambda(u) = \int_{-\infty}^{\infty} X(t)\psi_{\lambda,u}(t)\,dt. \tag{4}$$

$X'_\lambda(u)$ is called the wavelet transform of $X(t)$ at scale λ and location u. It is also called here the "local fluctuation" or "detail" process, compared to the process $\overline{X}_\lambda(u)$, which is called the "local average" process at scale λ and location u. Locality comes from the finite support of the filters $\phi_{\lambda,u}(t)$ and $\psi_{\lambda,u}(t)$.

Note that in the previous example (Figure 2) the scaling and wavelet functions (at scale $\lambda = 1$) were

$$\phi(t) = \begin{cases} 1 & 0 \le t < 1 \\ 0 & \text{otherwise,} \end{cases} \tag{5}$$

$$\psi(t) = \begin{cases} 1 & 0 \le t < \frac{1}{2} \\ -1 & \frac{1}{2} \le t < 1 \\ 0 & \text{otherwise} \end{cases} \tag{6}$$

which result in the Haar wavelet transform of a process. Construction of scale functions and wavelets other than the above is possible, e.g., the Daubechies wavelets which can be found in the work of *Daubechies* [1992].

For implementation of the wavelet transform on a sampled process $X(t)$, that is, a sequence of numbers $\{x_n\}_{n\in Z}$, the scale and location parameters can be discretized, giving rise to discrete wavelet transforms. For orthogonal wavelets, selection of dyadic scales $\lambda = 2^m$ (i.e., 2^{-m} samples per unit length) and location parameters as multiples of the sampling intervals $u = n\,2^m$ is convenient. Thus the discrete wavelet (discrete in scale and location but not in time) can be written as

$$\psi_{m,n}(t) = 2^{-m}\psi(2^{-m}t - n) \tag{7}$$

and the corresponding scaling function as

$$\phi_{m,n}(t) = 2^{-m}\phi(2^{-m}t - n) \tag{8}$$

where the parameter m corresponds to scale ($\lambda = 2^m$) and the parameter n corresponds to location. The discrete local average value at scale m and location n is then given as

$$\overline{X}_m(n) = \{\langle X, \phi_{m,n}\rangle\}_{n\in Z} \tag{9}$$

and the discrete wavelet coefficient at the same scale and location as

$$X'_m(n) = \{\langle X, \psi_{m,n}\rangle\}_{n\in Z} \tag{10}$$

where $\langle f, g\rangle$ denotes the inner product $\int_{-\infty}^{\infty} f(t)\overline{g}(t)\,dt$, and $\overline{g}(t)$ denotes the complex conjugate of $g(t)$.

The above results can easily be extended to a two-dimensional process $X(t_1, t_2)$ by applying the separable two-dimensional multiresolution framework [*Mallat*, 1989]. In this framework the scaling function is $\Phi(t_1, t_2) = \phi(t_1)\phi(t_2)$ and the three wavelet functions are $\Psi^1(t_1, t_2) = \phi(t_1)\psi(t_2)$, $\Psi^2(t_1, t_2) = \psi(t_1)\phi(t_2)$, and $\Psi^3(t_1, t_2) = \psi(t_1)\psi(t_2)$. In the discrete domain the discrete scaling function is defined as

$$\Phi_{m,n,k}(t) = 2^{-2m}\Phi(2^{-m}t_1 - n, 2^{-m}t_2 - k) \qquad (n, k) \in Z^2$$

and similar expressions hold for the discrete wavelet functions $\Psi^1_{m,n,k}(t)$, $\Psi^2_{m,n,k}(t)$, and $\Psi^3_{m,n,k}(t)$. Thus the two-dimensional discrete local average value at scale m and location (n, k) is given as

$$\overline{X}_m(n, k) = \{\langle X, \Phi_{m,n,k}\rangle_{(n,k)\in Z^2}\} \tag{11}$$

and the three wavelet coefficients at the same scale and location as

$$X'_{m,1}(n, k) = \{\langle X, \Psi^1_{m,n,k}\rangle_{(n,k)\in Z^2}\} \tag{12}$$

$$X'_{m,2}(n, k) = \{\langle X, \Psi^2_{m,n,k}\rangle_{(n,k)\in Z^2}\} \tag{13}$$

$$X'_{m,3}(n, k) = \{\langle X, \Psi^3_{m,n,k}\rangle_{(n,k)\in Z^2}\} \tag{14}$$

These three wavelet coefficients are directional; that is, they capture high frequencies of the process in the horizontal (index 1), vertical (index 2), and diagonal (index 3) directions of the frequency domain. Note, for example, that high frequencies in the horizontal direction of the frequency domain correspond to vertical edges in the original domain (i.e., high correlations in the vertical spatial direction; see for example *Kumar and Foufoula-Georgiou* [1993a] for more details). It is exactly these three components of equations (12), (13), and (14) that we extract from the spatial rainfall fields and we call "multiscale rainfall fluctuations" in the horizontal, vertical, and diagonal directions. In section 2.3 we give further interpretation to these components, and later we explore their scale-invariance properties.

2.3. Further Interpretation

Let us simplify the notation of the above processes by dropping the spatial location indices and referring to them as the multiscale average process $\overline{X}_m$ and the three multiscale fluctuation processes $\{X'_{m,i}\}_{i=1,2,3}$, where m refers to scale (recall $\lambda = 2^m$). The original process ($m = 0$) $X_0 \equiv \overline{X}_0$ is decomposed to the processes $\overline{X}_1$ and $\{X'_{1,i}\}_{i=1,2,3}$ ($m = 1$); then the process $\overline{X}_1$ to the processes $\overline{X}_2$ and $\{X'_{2,i}\}_{i=1,2,3}$ ($m = 2$) (see Figure 3). If the two-dimensional Haar wavelets are used for the decomposition, the rainfall fluctuation components admit an easy interpretation as gradients

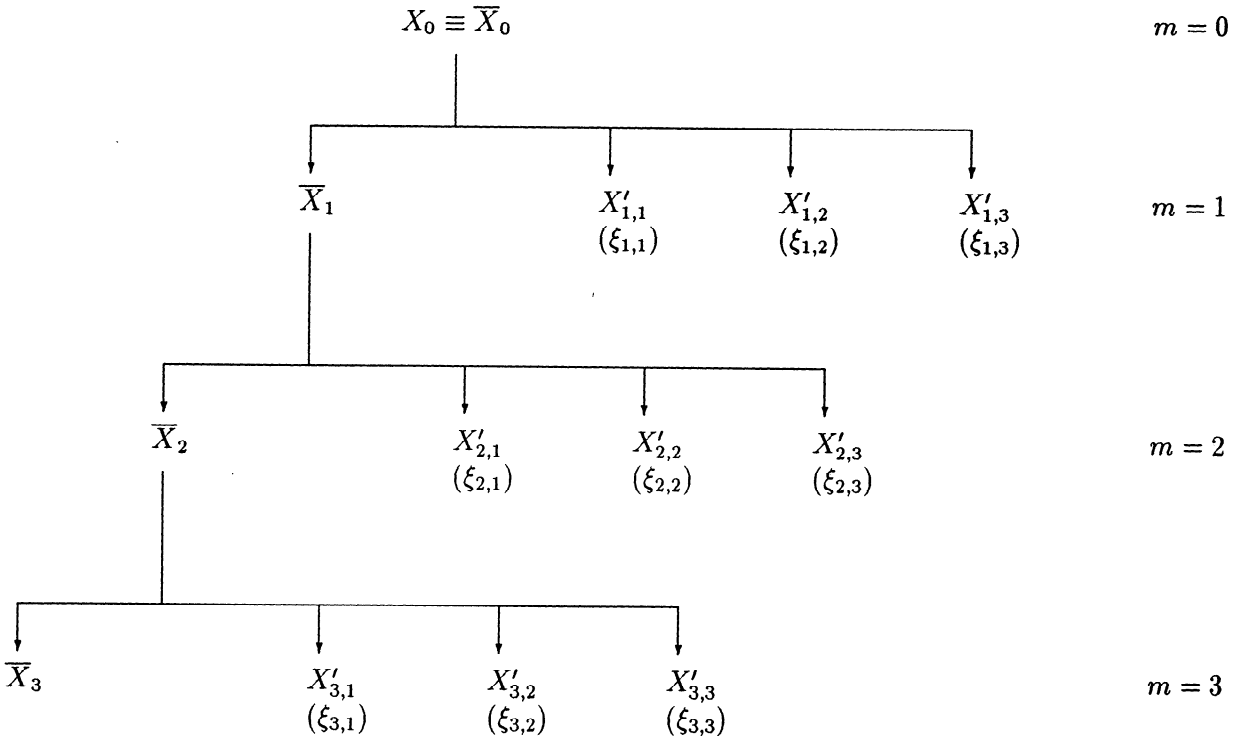

Figure 3. Schematic showing rainfall decomposition. $\overline{X}_m$ represents the average process at scale m, $X'_{m,i}$ represents the ith fluctuation component ($i = 1, 2, 3$), and $\xi_{m,i}$ represents the corresponding standardized fluctuation component ($\xi_{m,i} = X'_{m,i}/\overline{X}_m$) at the same scale.

of the rainfall field in the vertical, horizontal, and diagonal directions. Indeed, the Haar wavelet coefficients are computed as

$$X'_{m+1,1}(n,k) = \frac{1}{4}\{[\overline{X}_m(i,j) + \overline{X}_m(i,j+1)] - [\overline{X}_m(i+1,j) + \overline{X}_m(i+1,j+1)]\} \quad (15)$$

$$X'_{m+1,2}(n,k) = \frac{1}{4}\{[\overline{X}_m(i,j) + \overline{X}_m(i+1,j)] - [\overline{X}_m(i,j+1) + \overline{X}_m(i+1,j+1)]\} \quad (16)$$

$$X'_{m+1,3}(n,k) = \frac{1}{4}\{[\overline{X}_m(i,j) - \overline{X}_m(i+1,j)] - [\overline{X}_m(i,j+1) - \overline{X}_m(i+1,j+1)]\}. \quad (17)$$

Thus they can be interpreted as discrete representations of $\partial\overline{X}_m/\partial t_1$, $\partial\overline{X}_m/\partial t_2$, and $\partial^2\overline{X}_m/\partial t_1\partial t_2$, respectively, and as such they correspond to a scheme widely used for defining gradients of two-dimensional processes. The indices (i, j) define positions in t_1 and t_2 directions at scale m; (n, k) are indices at scale $(m+1)$. Notice that the number of grid points at a particular scale is reduced by a factor of 2 in each direction at the next larger scale. The average process at scale $(m+1)$, $\overline{X}_{m+1}(n,k)$, is computed as the averages of the appropriate mean rainfall values at the previous scale

$$\overline{X}_{m+1}(n,k) = \frac{1}{4}[\overline{X}_m(i,j) + \overline{X}_m(i+1,j) + \overline{X}_m(i,j+1) + \overline{X}_m(i+1,j+1)]. \quad (18)$$

It is important to emphasize that the processes $\{X'_{m+1,i}\}_{i=1,2,3}$ represent gradients of the previous-scale average process and not averages of the previous-scale gradient process; that is, as we increase scale, we smooth the process and look at the gradients of the progressively smoother process as opposed to forming the gradient process at the initial scale and then smoothing (by averaging) this gradient process over scales. In symbols, if $\Phi[X]$ denotes the application of the smoothing operator on the process X, and $\Psi[X]$ denotes the application of the differencing operator on the same process, then X'_{m+1} results from $\Psi[\overline{X}_m]$ and not from $\Phi[X'_m]$. The reason for emphasizing this distinction is to note that simple scaling (to be discussed in section 3) of fluctuations $X'_{m+1} = \Psi[\overline{X}_m]$ does not in any way imply simple scaling for either the original process X_0 or the fluctuation process X'_1.

3. Midlatitude Mesoscale Convective Systems

3.1. Data Sources

The principal source of data used in this study is the Oklahoma-Kansas Preliminary Regional Experiment for Storm-Central (PRE-STORM) field program. The main purpose of this experiment was to investigate the structure and dynamics of mesoscale convective systems ranging from multicell systems to mesoscale convective complexes. A number of sensing systems were used to collect the data. As part of the program, high density upper air soundings were taken at regular NWS sites as well as at eleven supplemental PRE-STORM sites. Soundings were released approximately every 3 hours and occasionally every 1.5 hours on selected operational days. Locations of the radar and sounding stations with their three-letter NSSL site identifiers are shown in Figure 4. Digitized volume-scan reflectivity data were available from Oklahoma and Kansas NWS WSR-57 radar sites. Each site recorded volume-scan radar data at each 2° radially with a gate spacing of 1 nm; volume scans were made at 2° increments up to a maximum height of 22°. Six volume scans per hour were possible (one scan every 10 min). See, for example, *Cunning* [1986] for more details.

For the purpose of our analysis we needed rainfall intensity data on the ground on rectangular grids. The conversion of the two-dimensional surface reflectivity fields to rainfall rates via appropriate Z-R relations and further conversion of the rainfall intensities from polar to rectangular grids, with horizontal grid increments of approximately 4 km (4.03 km for Oklahoma and 4.11 for Wichita), was done by the J.A. Smith group at Princeton University. A few hundred radar rainfall scans were collected during the 2-month PRE-STORM program, covering a broad spectrum of structural characteristics of rainfall events. To be able to perform a reasonably reliable scaling analysis, we were forced to restrict ourselves to radar scans for which rainfall events covered relatively large areas so that we had enough data for at least three to four spatial scales. Therefore our working sample consisted of 47 selected radar scans. It must be recognized that due to the above mentioned selection process, our analysis and results are mostly applicable to the mature and dissipating stages of storm development, where the areal extent of the event is usually much larger than during its formation stage.

3.2. Self-Similarity in Rainfall Fluctuations

On the basis of the analysis of a winter storm that occurred on February 22, 1985, and a heavy squall line storm which occurred on May 17, 1987, over Oklahoma, *Kumar and Foufoula-Georgiou* [1993b] suggested that rainfall fluctuations (as defined in section 2.2) may exhibit simple-scaling behavior up to a scale of approximately 50 to 60 km.

Simple scaling (self-similarity) is established if the finite-dimensional distribution functions of the process (in this case of the three rainfall fluctuation components $\{X'_{m,i}\}_{i=1,2,3}$) satisfy the following scaling condition:

$$\{X'_{m,i}\} \stackrel{d}{=} \{(2^{m-1})^{H_i} X'_{1,i}\} \qquad i = 1,2,3 \quad (19)$$

where H_i are the scaling exponents and $\stackrel{d}{=}$ stands for equality in distribution.

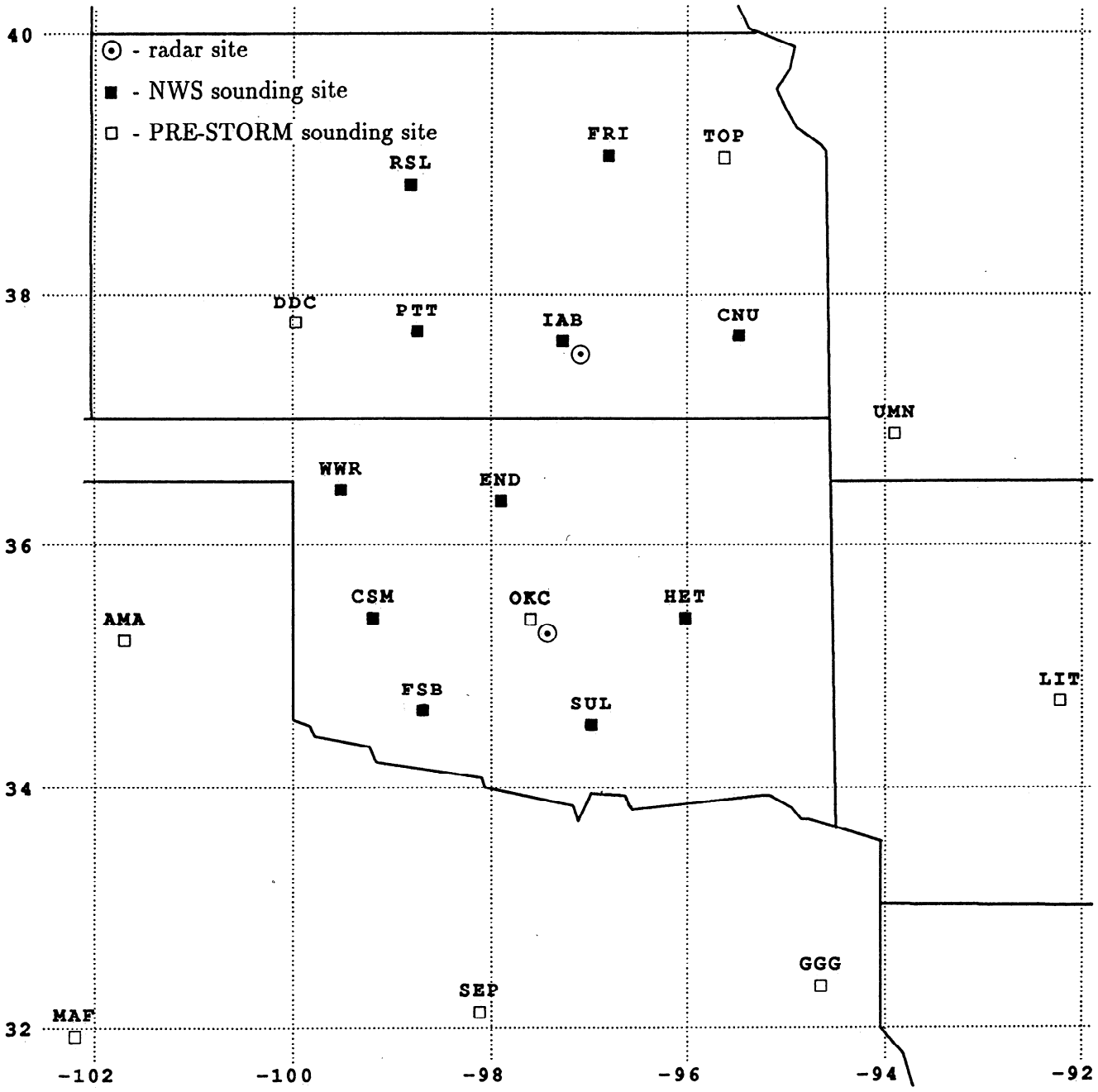

Figure 4. Oklahoma-Kansas Preliminary Regional Experiment for Storm-Central (PRE-STORM) sounding network.

We tested simple-scaling properties of rainfall fluctuations on 47 data sets from the PRE-STORM experiment, selected as described in section 3.1. To establish self-similarity in the sense of the above equation, the marginal distribution functions of $X'_{m,i}$ at all scales m for which self-similarity holds must be of the same type for each of the three components ($i = 1, 2, 3$). Based on our working sample, it was found that the appropriate probability density functions (pdfs) for all three components at all studied scales, i.e., all $\{X'_{m,i}\}_{(m\geq 1, i=1,2,3)}$, were symmetric, zero-median distributions with long tails. Among several commonly used symmetric, finite-moment distributions (Gaussian, t-distribution, etc.), none were capable of capturing as much variability of the empirical pdfs as stable distributions. Stable distributions, in general, are four-parameter distributions $\mathcal{S}(x; \alpha, \beta, \delta, c)$, where $0 < \alpha \leq 2$ is a characteristic exponent, $-1 \leq \beta \leq 1$ is a skewness or symmetry parameter, $-\infty < \delta < \infty$ is a location parameter, and $c > 0$ is a scale parameter. In the symmetric case ($\beta = 0$) this class includes the Cauchy ($\alpha = 1$) and Gaussian $\mathcal{N}(\alpha = 2, \mu = \delta, \sigma^2 = 2c^2)$ distributions. The characteristic function of the symmetric stable class is

$$\rho(\xi)|_{\beta=0} = \exp(i\delta\xi - |c\xi|^\alpha). \tag{20}$$

Symmetric stable distributions provided an excellent

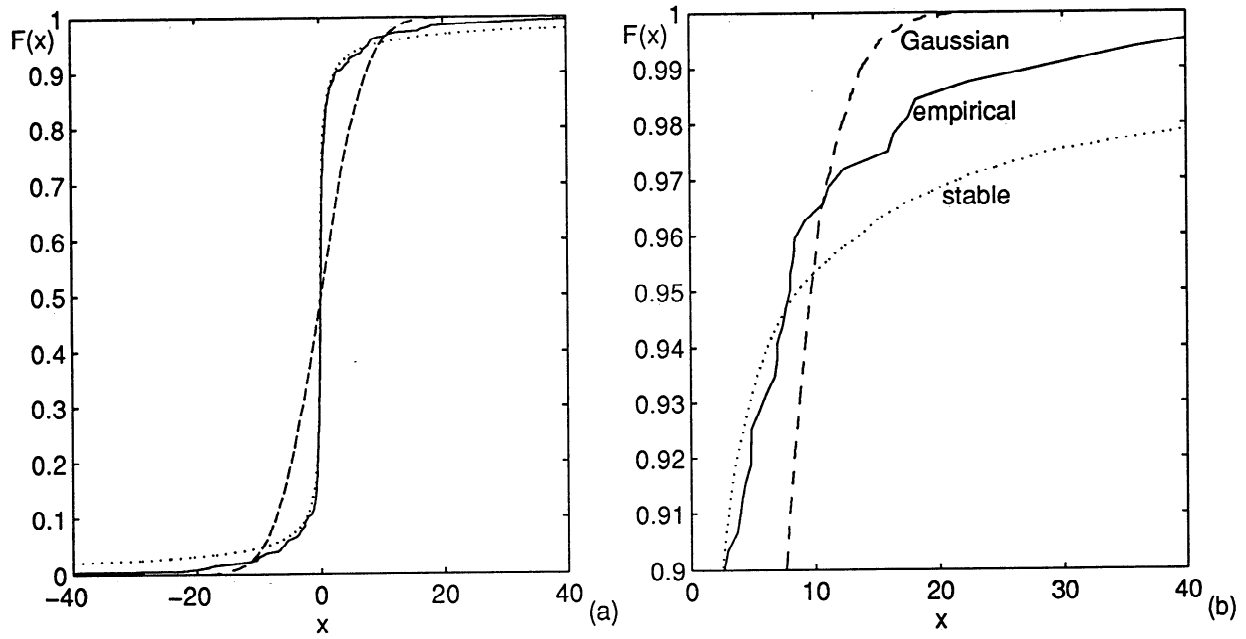

Figure 5. The 1248 UTC May 13, 1985, data set. Comparison between the performance of a Gaussian distribution $\mathcal{N}(\mu = 0.2, \sigma^2 = 33.5)$ and an estimated symmetric stable distribution $S(\alpha = 0.6, \delta = 0, c = 0.32)$ for the fluctuation component $X'_{1,1}$. (a) Cumulative distribution functions and (b) in detail the right tails of the distributions. The solid line corresponds to the empirical cdf, the dashed line to the Gaussian cdf, and the dotted line to the stable distribution.

fit for at least 90-95% of the body of the empirical distributions of $X'_{m,i}$. As an illustrative example, Figure 5 shows the performance of the estimated symmetric stable distribution with zero mode (parameters $\alpha = 0.6$, $\delta = 0$, and $c = 0.32$ were estimated by a method developed by *Arad* [1980]) and the estimated Gaussian distribution $\mathcal{N}(\mu = 0.2, \sigma^2 = 33.5)$, for comparison, for the fluctuation component $X'_{1,1}$ of the 1248 UTC May 13, 1985, data set. As is evident in this figure, the symmetric stable distribution provides a very good visual fit. It captures very well the empirical distribution from approximately the 5th to the 95th percentile but not so well the tails of the distribution (it has thicker tails compared to the empirical pdf, based here on 416 values). Note that the Gaussian distribution (or any other finite-moment distribution) is not able to capture well even the body of the empirical distribution. To further test the appropriateness of the stable distribution, some quantitative tests were applied. Since classical goodness of fit tests are not reliable for infinite-moment distributions (see *Granger and Orr* [1972] for discussion), other "descriptive tests" were applied, such as the "converging variance test" [*Granger and Orr,* 1972], the "converging mean test" [*Granger and Orr,* 1972], and the "tail test" [*Mandelbrot,* 1963]. Regularly, some of these tests failed and some passed, making it difficult to conclusively establish the stability of the $X'_{m,i}$ distributions.

Even in the cases where the estimated stable distributions "passed" the above mentioned tests, the eventual simple-scaling nature of each fluctuation component would be established only if the value of the parameter α was found to be the same for all scales m over which self-similarity holds. However, it was found that variations observed in the estimated characteristic exponents $\alpha_{m,i}$ over the available range of scales were too significant to be ignored (Figures 6a, 6c, 6e). Moreover, for symmetric stable distributions with zero mode, the scaling condition (19) results in

$$c_{m,i} = 2^{(m-1)H_i} c_{1,i} \qquad i = 1, 2, 3 \qquad (21)$$

where $c_{m,i}$ are the scale parameters for each fluctuation component ($i = 1, 2, 3$) at the range of scales m at which self-similarity holds. Therefore power-law behavior of the scale parameters with scale is needed to establish the scaling nature of fluctuations, if it exists. However, the scaling coefficients $c_{m,i}$ did not follow power-law behavior over scales but rather changed almost randomly (Figures 6b, 6d, 6f). Figure 6 illustrates a typical example of the obtained results; similar results were obtained for other radar scans of the same storm and other storms.

3.3. Gaussianity and Self-Similarity of Standardized Fluctuations

Because of the properties of orthogonal wavelet transforms, the scale coefficients representing the local mean rainfall rates $\overline{X}_m$ and the corresponding wavelet coefficients representing rainfall fluctuations $\{X'_{m,i}\}_{i=1,2,3}$ at the same scale m are uncorrelated. However, for rainfall

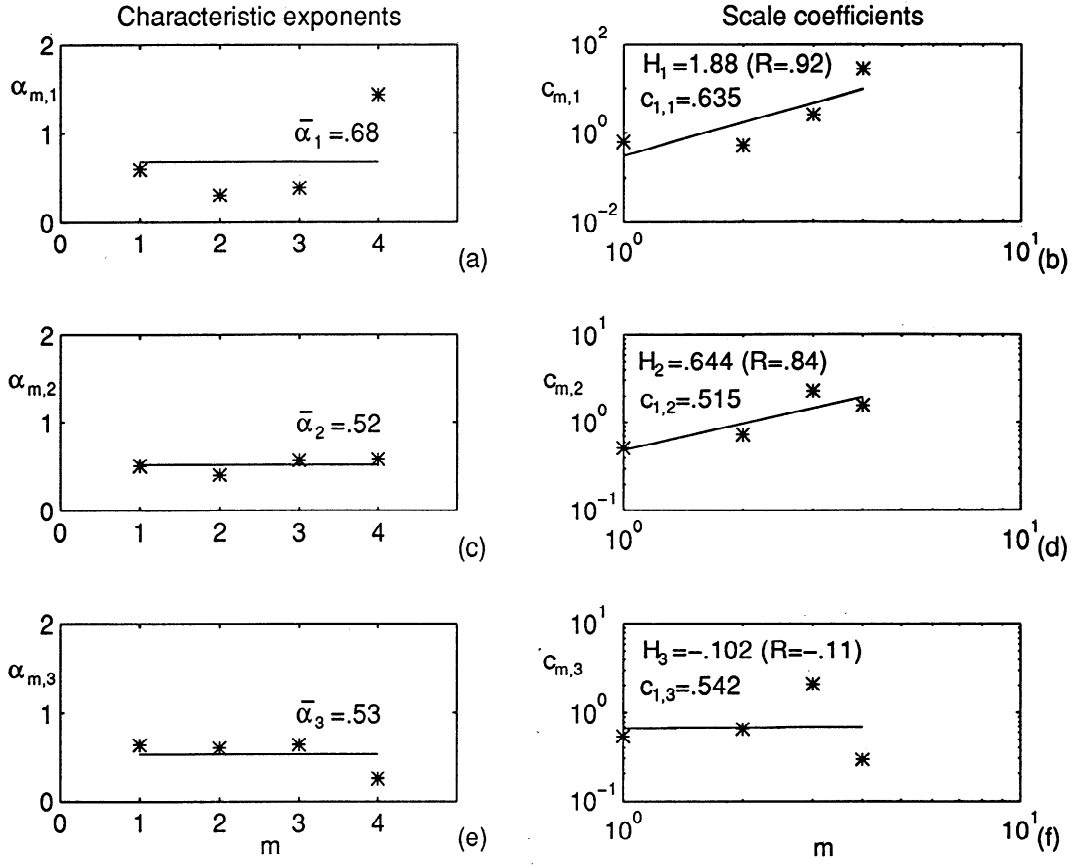

Figure 6. The 1248 UTC May 13, 1985, data set. (a, c, and e) Estimated characteristic exponents $\alpha_{m,i}$ with respect to scale m for the three fluctuation components $X'_{m,1}$, $X'_{m,2}$, and $X'_{m,3}$, respectively. The mean values $\overline{\alpha}_i$ are also indicated in the figures. (b, d, and f) Log-log plots of the scale parameters $c_{m,i}$ versus scale m for the same components. The values of the scaling exponents H_i, scale parameters $c_{1,i}$, and coefficients of correlation R for each regression line are also indicated in the figures.

fields a strong linear dependence between the absolute values of fluctuations and the corresponding local means was found to exist. Figures 7a and 7b show scattergrams of $X'_{1,1}$ versus $\overline{X}_1$ and $|X'_{1,1}|$ versus $\overline{X}_1$ with the regression lines and correlation coefficients ($R = 0.05$ and $R = 0.81$, respectively) for the 1248 UTC May 13, 1985, radar scan. The strong linear dependence of $\overline{X}_m$ and $|X'_{m,i}|$ indicates that when the local average rainfall rate is large, so is the gradient (in absolute value) of the rainfall rate (see interpretation of rainfall fluctuations in section 2). This observation prompted us to look at the "standardized rainfall fluctuations" obtained from rainfall fluctuations by dividing them by their corresponding local means; that is,

$$\xi_{m,i} = \frac{X'_{m,i}}{\overline{X}_m}. \tag{22}$$

This standardization contributed to reducing the thick tails of $X'_{m,i}$, and it was found that the Gaussian distribution, or a stable distribution very close to it (i.e., characteristic exponents of estimated stable distributions $\alpha_{m,i}$ were regularly equal to 2 and never lower than 1.9), provided an excellent fit to the $\xi_{m,i}$ for the majority of the data sets. Figure 8 provides a typical example of the performance of the Gaussian distribution for the standardized fluctuation components $\{\xi_{1,i}\}_{i=1,2,3}$ at scale $m = 1$ for the 1248 UTC May 13, 1985, data set, used here as an illustrative example. Similar results hold for the other scales and other radar scans of the same storm and other storms. It seems that owing to the fact that the mean rainfall intensities themselves possess long tails and positive behavior, the long tails observed in the fluctuations were reduced to Gaussian tails after standardization.

The standardized fluctuations exhibited very good simple scaling behavior for all analyzed data sets: the coefficients $\alpha_{m,i}$ were practically constant over all tested scales and regularly equal to 2, and log-log linearity of $c_{m,i}$ versus m held quite well (correlation coefficients were almost always greater than 0.9). Figure 9 shows as an example the results of the scaling analysis for the 1248 UTC radar scan of the May 13 storm event. Scaling was found present over the whole range of tested scales, corresponding to grid increments of 8 to 64 km

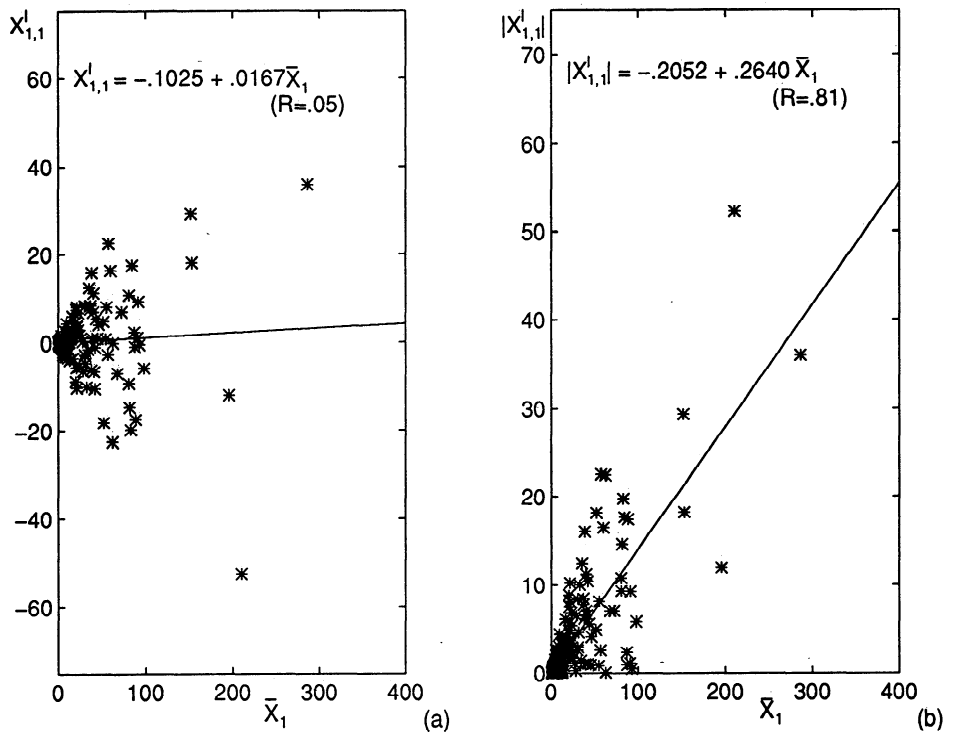

Figure 7. The 1248 UTC May 13, 1985, data set. (a) Plot of the rainfall fluctuation component $X'_{1,1}$ versus $\overline{X}_1$ and (b) plot of the absolute values $|X'_{1,1}|$ versus $\overline{X}_1$ (number of data pairs N=416). Regression lines and correlation coefficients are also indicated in the figures.

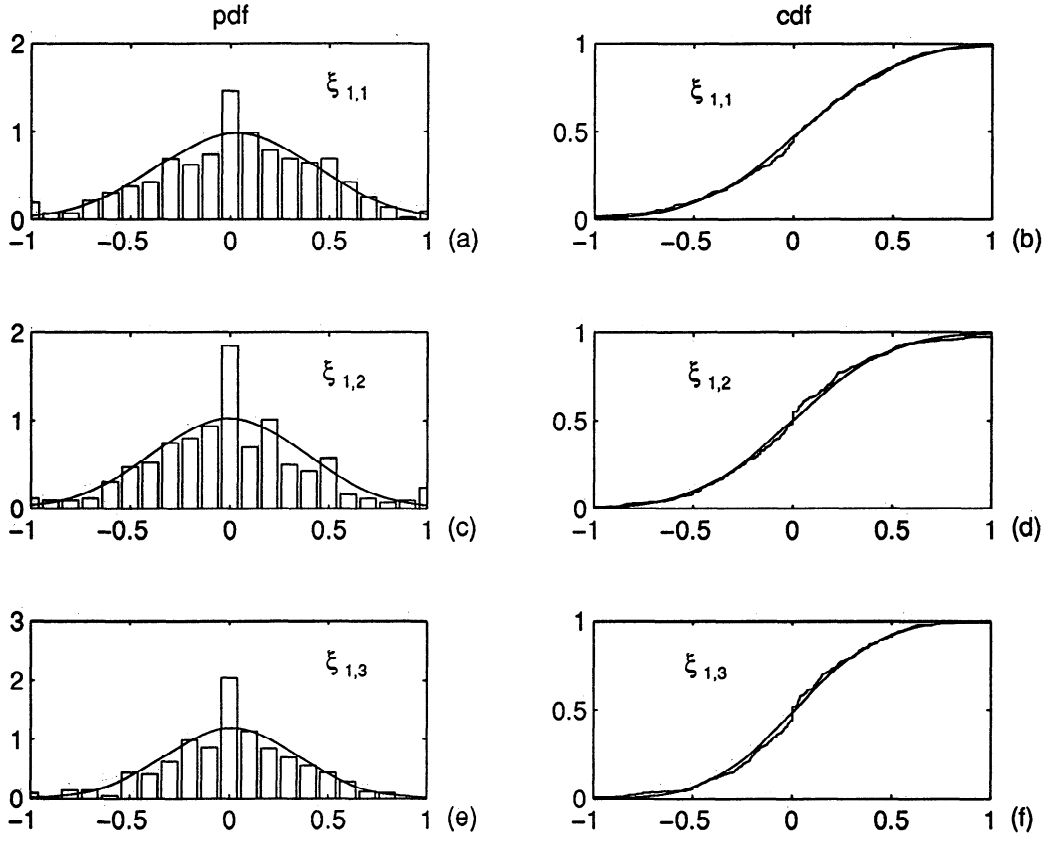

Figure 8. The 1248 UTC May 13, 1985, data set. (a, c, and e) Comparison between empirical and estimated Gaussian pdf values. (b, d, and f) Comparison between empirical and Gaussian cumulative distributions for the standardized fluctuation components $\{\xi_{1,i}\}_{i=1,2,3}$, at scale $m = 1$.

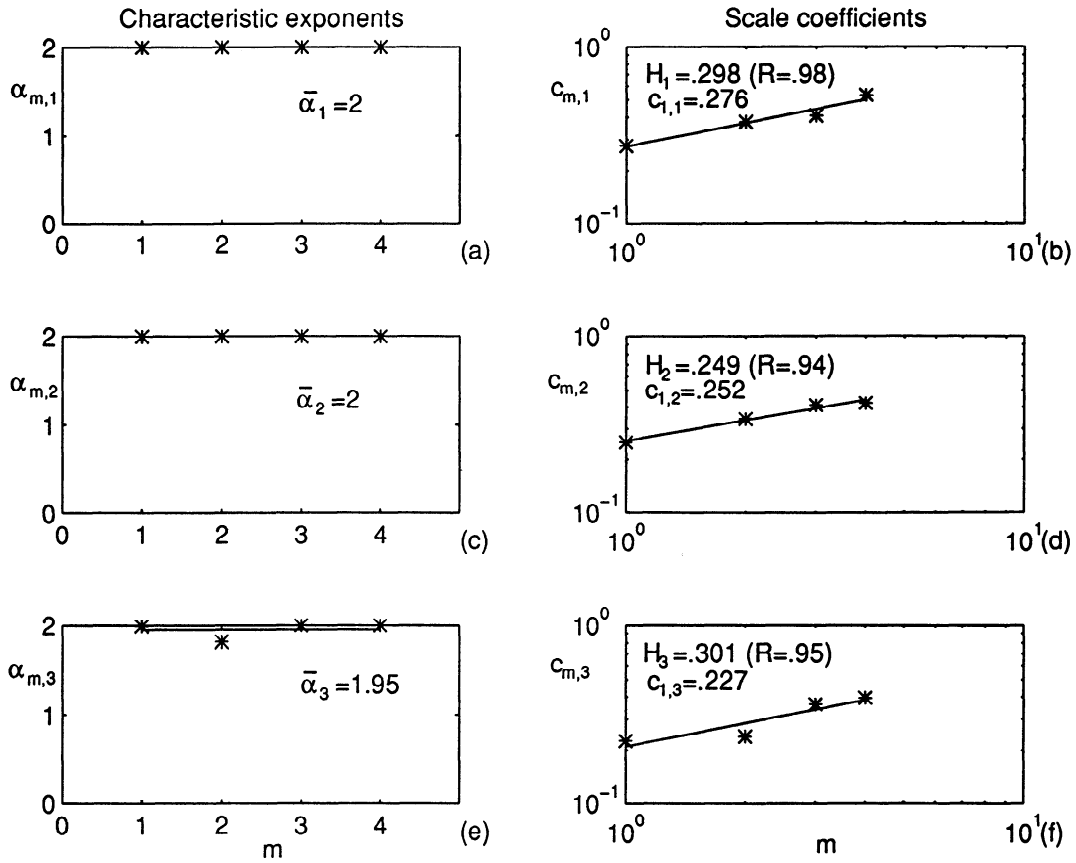

Figure 9. Same as Figure 6 but for standardized fluctuations.

(limitations on the range of scales considered were due to data availability). Similar results were found for all other radar scans of this and other storms.

The fact that standardized fluctuations are described by simple-scaling Gaussian distributions resulted in their parameterization with six parameters, two for each fluctuation component: $\{H_i, c_{1,i}\}_{i=1,2,3}$. (Note that the parameters H_i are scale invariant, while the parameters $c_{1,i}$ refer to the first scale $m = 1$ (here 8×8 km); parameters $c_{m,i}$ at other scales are obtained from $c_{1,i}$ and H_i based on equation (21).) Another advantage of dealing with standardized fluctuations, instead of dealing with fluctuations themselves (which if found stable and simple scaling would need nine parameters to be characterized: $\{\alpha_i, H_i, c_{1,i}\}_{i=1,2,3}$), is related to reduction of bias in radar-rainfall estimates. It is well known that the Z-R relations used for converting radar reflectivities into rainfall intensity rates are subject to large uncertainties. For testing purposes we used several relations (or combinations of two different relations for stratiform and convective portions of the event separately) to produce a wide range of rain rate estimates for the same reflectivity fields. We found that the scaling parameterization of fluctuations (overlooking for a moment that simple scaling was not found present in most fluctuations) was sensitive to the particular Z-R relationship used. However, due to the strong relation between mean rainfall intensities and corresponding fluctuations, their ratios, representing standardized fluctuations $\xi_{m,i}$, had significantly reduced bias. Therefore inferences about scaling and estimates of the scaling parameters were rather insensitive to the Z-R relationship used.

Another important issue to be discussed here is the choice of analyzing wavelet and the sensitivity of the results to that choice. The Haar wavelet was chosen in our analysis due to its simplicity and the appealing physical interpretation of the obtained wavelet coefficients as directional gradients of the rainfall fields. Besides, as argued by *Kumar and Foufoula-Georgiou* [1993a], it is probably adequate for rainfall description since other authors [e.g., *Barancourt et al.*, 1992], have reported independently that intrinsic random functions of zero order provide an adequate description of the spatial mean behavior of rainfall. Despite these arguments, we still proceeded with the application of other smoother wavelets (i.e., the *Daubechies* [1992] wavelets D4 and D6, which have two and three vanishing moments, respectively). These wavelets result in average and fluctuation components which can be interpreted as generalized rainfall averages and generalized rainfall fluctuations, i.e., they use different weights for adjacent observations and typically involve more surrounding values since they have larger supports. We found that the results, i.e., inferences about scaling in stan-

dardized fluctuations and estimates of scaling parameters, were not sensitive to the choice of wavelets. This gives us more confidence to proceed with seeking interpretations and connections of the scaling parameters with physical parameters of the storm environment.

3.4. Scaling Parameterization As Function of the Type of the Storm System

One of the objectives of this study was to explore whether the proposed scaling parameterization for standardized fluctuations depends on the storm type. For this purpose we classified storm systems as either stratiform or convective, based on the dominant precipitation mechanisms. Among convective systems, a distinction was made between linear (squall line) and all other systems that do not exhibit linear structure, termed chaotic [*Blanchard,* 1990]. First, we found that scaling of standardized rainfall fluctuations was present over the same range of scales (8 to 64 km), independent of storm type. Second, we found that for stratiform systems the estimated H_i values were in the range of 0.14-0.18 and the estimated $c_{1,i}$ values were in the range of 0.3-0.4. For convective systems the H_i values were higher (approximately 0.2-0.45) and the $c_{1,i}$ values were lower (in the range of 0.1 to 0.35). Among convective systems, we could not clearly distinguish differences in the parameters of chaotic and linear systems. The scaling parameters were found to be more dependent on the intensity of convective instability of the prestorm environment than on the specific storm type (chaotic versus linear convective); storms in areas of greater convective instability had higher H and smaller c estimates. The other important finding was that for linear systems, which are highly anisotropic, the estimated parameters were found to depend only slightly on direction. For stratiform and chaotic convective systems these differences were almost insignificant, apart from a few cases where estimates of H_3 and $c_{1,3}$ for the ξ_3 component deviated significantly from the parameter estimates for ξ_1 and ξ_2. These findings have significant implications for a subgrid-scale parameterization model. They indicate that (1) no distinction is needed between linear and chaotic storm types and (2) that the estimated scaling parameters may be assumed to be the same in all directions. These assumptions significantly improve the parsimony of the model, as demonstrated by *Perica* [1995].

The above statistical findings are physically interpretable. For example, the slight directionality of the scaling parameterization found in highly anisotropic linear convective systems is a direct result of the pronounced anisotropy in rainfall intensities which (by taking differences of adjacent values and dividing by the corresponding means) propagates only to a small degree in the corresponding standardized rainfall gradients. Also, the lower values of $c_{1,i}$ in convective systems, compared to those in stratiform systems, are directly related to the much lower rainfall gradients relative to their corresponding averages, which in turn results in a small variability in standardized fluctuations. More detailed interpretations are provided in section 4, where quantitative measures of storm system environments are introduced and are connected to the scaling parameterization.

4. Relation Between Scaling Parameters and Parameters Describing the Storm Environment

The hypothesis was set forward that the developed parameterization, since it is scale invariant, might be connected to physical characteristics of the storm. The validity of this hypothesis is tested in this section using a dense network of PRE-STORM rawinsonde stations, coupled with regular NWS sites, which gave us an opportunity to estimate relevant environmental parameters for storms for which radar data were also available.

The selection of soundings used to find representative environmental characteristics was based on the location of the sounding site with respect to the storm system. Our intent was to establish a working sample that included data sets for which a relatively synchronous collection of radar rainfall intensities and soundings taken at locations ahead of the storm system were available. Soundings that appeared to be contaminated by convection or that were far ahead of the storm were excluded. To address the environmental conditions supporting the mesoscale convective events and to check them for possible relations with scaling parameterization, a number of parameters measuring atmospheric stability and forcing were used. When more than one sounding was available, parameters computed from selected individual soundings were averaged to produce representative environmental characteristics. Computation of quantities derived from the soundings was done by using the *General Meteorological Package (GEMPAK)* [1992]. Since it is outside the scope of this paper to define all those parameters, the reader is referred to the *GEMPAK* manual or other journal papers [e.g., *Bluestein and Jain,* 1985; *Houze et al.,* 1990] for their definition. Measured surface pressure along with the average potential temperature and mixing ratio in the lowest 50 mbar were used to define characteristics of the surface parcel used in computing stability indices. In Table 1 we list all parameters employed in the analysis, along with their units and symbols used further in the text.

On the basis of the above selection criteria our working sample for relating scaling parameters to storm environmental characteristics consisted of 17 data sets, or approximately 30% of the total number of cases studied for self-similarity. Table 2 lists the time of occurrence of these events as well as identifiers for the locations of the soundings used to produce the averaged parameters. Table 3 summarizes the calculated thermodynamic and kinematic parameters used for establishing relations with the statistical parameterization.

Table 1. List of All Environmental Parameters Used in the Analysis Together With Units and Symbols

Symbol	Parameter	Units
CAPE	convective available potential energy	$m^2\ s^{-2}$
CIN	convective inhibition	$m^2\ s^{-2}$
CT	cross totals index	°C
EL	equilibrium level	mbar
K index	K index	°C
LFC	level of free convection	mbar
LI	lifted index	°C
PW	precipitable water	mm
Ri	bulk Richardson number	(dimensionless)
$S_{0-2.5}$	wind shear magnitude in layer surface–2.5 km	$10^{-3}\ s^{-1}$
$S_{2.5-6}$	wind shear magnitude in layer 2.5–6 km	$10^{-3}\ s^{-1}$
S^2	wind shear energy	$m^2\ s^{-2}$
Show	Showalter index	°C
SWEAT	SWEAT index	(dimensionless)
TT	total totals index	°C
VT	vertical totals index	°C
u_0	u component of the wind at surface	$m\ s^{-1}$
v_0	v component of the wind at surface	$m\ s^{-1}$
$u_{0-2.5}$	mean u component of the wind in layer surface-2.5 km	$m\ s^{-1}$
$v_{0-2.5}$	mean v component of the wind in layer surface-2.5 km	$m\ s^{-1}$

Regression analysis was used to quantify relations between the environmental parameters in Table 3 and the scaling parameters of spatial standardized rainfall fluctuations. For most of the storm systems directionality was not pronounced; thus the relations between environmental parameters and mean scaling parameters $\overline{H} = \sum_{i=1}^{3} H_i/3$ and $\overline{c}_1 = \sum_{i=1}^{3} c_{1,i}/3$ were examined. The best relations were obtained with the convective available potential energy (CAPE) values:

$$\overline{H} = 0.0516 + 0.9646(\text{CAPE} \times 10^{-4}) \quad (23)$$

$$\overline{c}_1 = 0.3811 - 0.6029(\text{CAPE} \times 10^{-4}) \quad (24)$$

with correlation coefficients of $R = 0.82$ and $R = -0.73$, respectively. These relations imply that a single thermodynamic parameter is capable of explaining approximately 60% of the variance of both scaling parameters $\overline{H}$ and $\overline{c}_1$. The scattergram of CAPE and $\overline{H}$ with the best fit least squares regression line is shown in Figure 10a, and that of CAPE and $\overline{c}_1$ is shown in Figure 10b.

Another supportive relation was found between the equilibrium level (EL) and $\overline{H}$ and $\overline{c}_1$ (with $R = -0.59$ and $R = 0.66$, respectively). Correlation existed between the lifted index (LI) and $\overline{H}$ ($R = -0.48$). However, the correlation between LI and $\overline{c}_1$ was low ($R = 0.16$). When two events from the May 20, 1985, storm (1936 and 2100 UTC) were removed, good correlation was obtained between the Showalter index (Show) and $\overline{H}$ ($R = -0.59$). Without the 1200 UTC May 13 event, the correlation coefficient between the precipitable water (PW) and $\overline{H}$ was $R = 0.67$, and with $\overline{c}_1$ it was $R = -0.53$. The exclusion of these events was based solely on improving the empirical linear relationships.

The nondimensional bulk Richardson number (Ri) is a very popular parameter since it combines information

Table 2. Date and Time of Occurrence of Selected Radar Scans

Event	Date	UTC	Site Identification		
1	May 13	1200	OKC		
2	May 20	1930	SUL		
3	May 20	2100	OKC		
4	June 4	0900	END		
5	June 4	2100	HET	SUL	
6	June 10	1800	OKC		
7	June 11	0000	DDC	PTT	
8	June 11	0300	END		
9	June 11	0430	HET	OKC	
10	June 11	0600	HET	SUL	
11	June 15	0600	END		
12	June 22	0600	END	FSB	
13	June 26	2100	CSM	END	
14	June 26	2230	CSM	CNU	
15	June 27	0000	CNU	FSB	OKC
16	June 27	0130	FSB	HET	
17	June 27	0300	HET		

The site identifications correspond to locations at which soundings were used for calculating average environmental parameters.

Table 3. Averaged Values for Environmental Parameters Calculated From Soundings at Locations As Listed in Table 2

	Event																
	1	2	3	4	5	6	7	8	9	10	11	12	13	14	15	16	17
Thermodynamic																	
CAPE($\times 10^2$)	24.8	10.3	10.2	18.6	21.4	14.3	14.4	20.8	23.4	21.2	19.0	19.1	16.0	12.6	14.7	19.7	15.8
CIN($\times 10$)	10.2	1.0	2.1	11.7	0.2	11.2	11.4	5.4	8.7	7.8	22.1	10.6	1.8	1.1	1.2	2.8	4.0
CT	28.9	29.0	27.4	26.1	23.8	18.9	26.0	23.8	23.6	24.2	24.6	25.9	19.5	21.1	22.1	22.6	23.2
EL($\times 10$)	19.6	21.6	23.1	16.3	15.3	16.2	16.6	12.7	13.9	14.0	17.0	17.3	17.2	17.7	16.0	15.4	17.1
K index	25.2	43.3	33.7	41.8	34.4	28.5	41.0	43.9	36.3	28.5	35.7	45.3	37.5	35.9	37.1	35.2	30.6
LFC($\times 10$)	69.3	83.7	69.0	75.9	78.1	69.2	68.7	80.6	75.3	78.6	72.9	70.5	78.7	84.5	84.2	78.6	78.0
LI	-6.1	-5.3	-4.4	-6.8	-5.3	-3.3	-6.1	-5.8	-5.3	-5.7	-7.1	-6.1	-2.5	-2.6	-3.7	-3.7	-3.4
PW	27.7	38.6	33.7	47.7	47.7	40.5	44.5	54.0	45.0	42.6	36.8	46.8	40.4	45.4	46.7	45.0	44.0
Show	-7.8	-6.8	-5.1	-6.3	-3.5	-0.1	-6.4	-4.3	-4.0	-4.0	-5.9	-6.3	0.1	-0.8	-1.9	-2.6	-2.7
TT	58.4	58.2	55.5	56.8	49.8	47.1	55.2	52.7	52.1	52.2	57.1	55.0	45.0	44.1	46.8	47.9	47.9
VT	29.5	29.2	28.1	30.7	26.0	28.2	29.2	28.9	28.6	28.0	32.5	29.1	25.3	23.0	24.8	25.3	24.6
Kinematic																	
$S_{0-2.5}$	3.4	6.5	5.6	7.3	5.6	5.2	9.5	5.6	5.3	6.2	3.8	5.2	3.9	4.6	4.9	3.9	2.9
$S_{2.5-6}$	3.3	5.1	4.5	0.9	3.3	3.7	4.5	3.4	4.5	3.6	6.9	3.5	2.1	1.6	2.5	1.4	1.9
S^2	21.1	66.3	62.4	22.2	24.2	53.5	95.0	42.9	44.1	33.1	65.3	49.4	1.4	14.4	5.8	4.6	14.6
u_0	-1.0	-0.9	-1.7	-3.0	0.0	-7.0	-6.1	-1.5	-0.9	0.3	-5.9	-1.0	1.0	0.8	2.1	-0.1	0.0
v_0	5.9	-0.3	4.7	-0.5	6.0	0.0	5.7	2.6	2.9	1.4	-1.0	2.8	6.8	8.4	0.8	0.5	0.0
$u_{0-2.5}$	5.8	0.1	5.7	3.5	5.7	-0.4	-3.2	4.7	8.3	10.3	14.1	6.1	5.0	6.8	5.5	5.2	4.2
$v_{0-2.5}$	13.8	8.3	3.5	17.9	12.2	7.9	14.6	10.3	7.5	9.4	4.5	7.1	2.8	8.2	7.1	6.1	4.7
Combined																	
Ri($\times 10$)	11.7	1.6	1.6	8.4	8.8	2.7	1.5	4.8	5.3	6.4	2.9	3.9	99.8	8.7	25.3	42.5	10.9
SWEAT($\times 10$)	48.7	41.6	35.2	46.7	33.6	19.7	42.2	32.2	30.7	31.4	44.8	38.8	23.4	25.8	25.5	24.3	23.8

from both thermodynamic and kinematic soundings. However, variations in *Ri* were too large for obtaining good correlations. The value of *Ri* deviates significantly for nonsevere systems: it can be extremely large when vertical wind shear is small and CAPE large, or extremely small for the opposite case. Even when only severe storms were used in the analysis, *Ri* was found to be only weakly correlated with $\overline{H}$ and $\bar{c}_1$ ($R \approx 0.3$). Among kinematic parameters, the only promising relation was found with $u_{0-2.5}$ ($R = 0.41$ and $R = -0.53$, respectively). Table 4 summarizes all obtained correlation coefficients.

Multilinear regression analysis was also performed to improve the correlation between scaling and environmental parameters and to allow the incorporation of directional relations for convective systems with significant anisotropy. However, none of the introduced parameters significantly improved the previously obtained correlations with CAPE. Regarding directionality, since the u and v components of the wind velocity are the only "parameters" specifically linked to directions (t_1 and t_2 in our case), they were an obvious choice for deriving appropriate "directional" regression equations for anisotropic convective systems. Again, no significant improvement was achieved; correlation coefficients obtained between each H_i and $c_{1,i}$ ($i = 1, 2, 3$) and CAPE improved at most by a few percent when u_0 and v_0 or $u_{0-2.5}$ and $v_{0-2.5}$ were included in the regressions. We concluded therefore that CAPE alone is a good predictor of the scaling structure of standardized rainfall fluctuations.

The positive correlations between CAPE and $\overline{H}$ and negative correlations between CAPE and $\bar{c}_1$ are explainable based on physical and statistical arguments. It is known, for instance, that there exist positive correlations among the maximum and mean rainfall rates and the corresponding measures of convective energy [e.g., *Zawadzki and Ro,* 1978; *Zawadzki et al.,* 1981]. In general, high CAPE values coincide with high observed rainfall intensities. It is also well known that there exists a strong spatial dependence in observed rainfall rates, i.e., high rainfall intensities are more likely to occur in the neighborhood of pixels with high intensity, which implies relatively small gradients (fluctuations) of the field. In general, this results in small variability of the rainfall fluctuations and, since the fluctuations are symmetric around zero mean, in small absolute values of the fluctuation processes $X'_{m,i}$ relative to the vari-

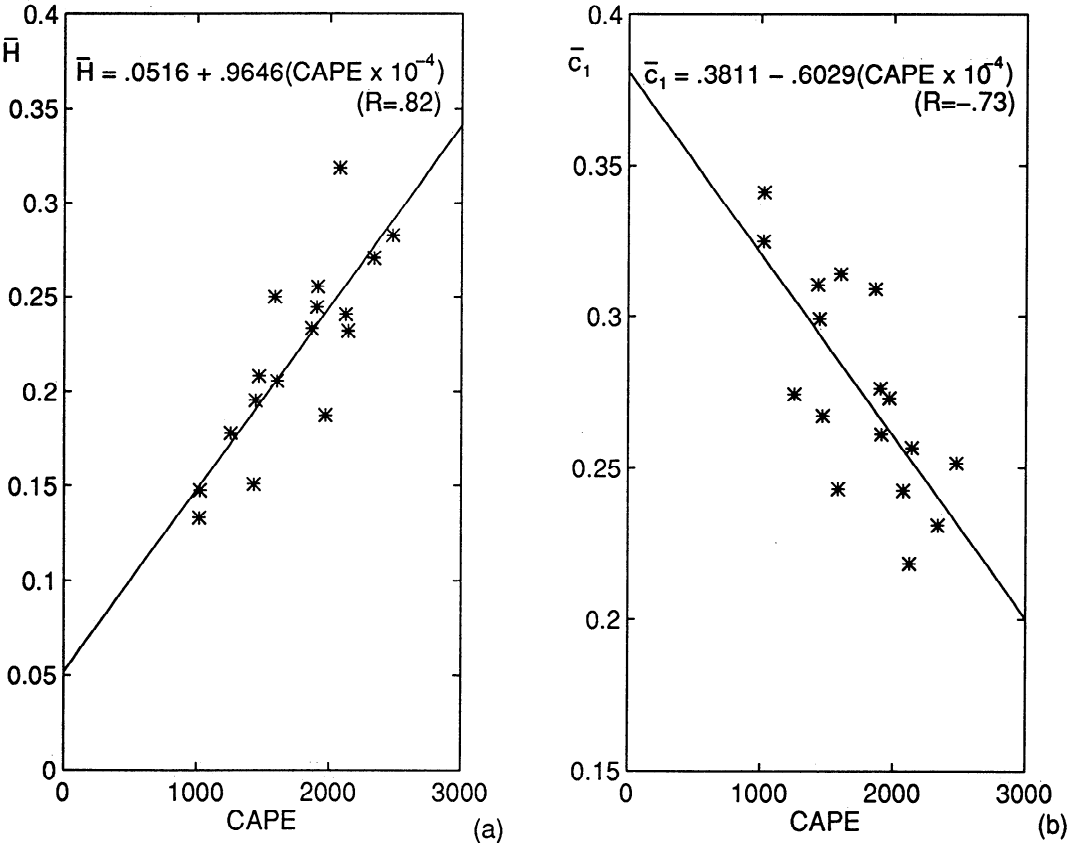

Figure 10. Scattergrams with indicated regression lines and correlation coefficients of (a) convective available potential energy (CAPE) and $\overline{H}$ and (b) CAPE and $\overline{c}_1$.

ability of the corresponding averaged process $\overline{X}_m$ at the same scale. This difference is much more pronounced for storms with high intensities than for the low-intensity storms. For example, as is noticeable from Figure 7, the rainfall intensities $\overline{X}_1$ are about 10 times higher than the rainfall gradients in the t_1 direction (i.e., $X'_{1,1}$) for the 1248 UTC May 13, 1985, radar scan. Having in mind that the standardized fluctuations are defined as the ratios between the fluctuations and the corresponding average field ($\xi_{m,i} = X'_{m,i}/\overline{X}_m$) and that these fields are highly dependent, the variability of the standardized fluctuations at scale $m = 1$ described through parameters $c_{1,i}$ (and equivalently their average value $\overline{c}_1$) is in general lower for higher-intensity storms. Therefore since storms with high rainfall rates have smaller $\overline{c}_1$ estimates and higher CAPE estimates, it follows directly that the correlation between CAPE and $\overline{c}_1$ values is negative. As we proceed with averaging of the rainfall process at larger scales $m > 1$, the differences between the average $\overline{X}_m$ and the gradients $X'_{m,i}$ at the same scale decrease. Accordingly, that implies higher dispersion in the probability density functions of the standardized fluctuations and higher $\overline{c}_m$ estimates. Differences in $\overline{c}_m$ estimates between storms with different intensities become less and less noticeable as we go to larger scales (notice that this also implies weaker correlation between $\overline{c}_m$ and CAPE for $m > 1$). The change of variability of the $\xi_{m,i}$ distributions as scale increases is more pronounced for highly convective storms. Equivalently, the scaling exponents H_i which explain the change in variability of $c_{m,i}$ over scales (i.e., are the slopes of the regression lines in the log-log diagrams of $c_{m,i}$ versus m) as well as their average value $\overline{H}$ have higher values for highly convective storms. Therefore the correlation between CAPE and $\overline{H}$ is positive.

It is noteworthy to mention that apart from being interesting in their own right, equations (23) and (24) are envisioned to be useful in a predictive mode, i.e., predict $\overline{H}$ and $\overline{c}_1$ based on values of CAPE. Since $\overline{H}$ and $\overline{c}_1$ together with a known large-scale average rainfall intensity permit (via inverse wavelet transform) to reconstruct the variability of the rainfall process at any desired small scale, these predictive equations can form the basis of a physical-statistical subgrid-scale parameterization scheme [see *Perica*, 1995]. In that case, care must be exercised as some additional conditions, not explicit in those equations, must be satisfied. For example, the above relations were based on 17 convective events which did occur and for which the negative area below the level of free convection was sufficiently small so it could be overgrown. Therefore the convective inhibition (CIN) as a measure of that negative area had

Table 4. Correlation Coefficients Between Environmental and Scaling Parameters

Parameter	Correlation Coefficient	
	$\overline{H}$	$\bar{c}_1$
CAPE	0.82	-0.73
CIN	0.32	-0.10
CT	0.11	0.11
EL	-0.59	0.66
K index	0.05	0.29
LFC	0.00	-0.12
LI	-0.48	0.16
PW	0.29 (0.67)	-0.30 (-0.54)
Show	-0.28 (-0.59)	-0.02 (0.24)
TT	0.20	0.14
VT	0.25	0.14
$S_{0-2.5}$	-0.21	0.30
$S_{2.5-6}$	-0.04	0.09
S^2	-0.20	0.31
u_0	0.14	-0.34
v_0	-0.02	-0.03
$u_{0-2.5}$	0.41	-0.54
$v_{0-2.5}$	0.24	0.10
Ri	-0.08	0.19
SWEAT	0.25	0.13

Numbers in parentheses represent improved coefficients when one or at most two of the 17 events were considered "outliers" and removed.

a small value relative to CAPE in all analyzed cases. This has to be the case for any storm for which equations (23) and (24) are to be applied in a predictive mode.

4.1. Parameterization Over Time

The ability of the obtained predictive relationships, between CAPE and $\overline{H}$ and between CAPE and $\bar{c}_1$ to predict the evolutionary statistical/scaling structure of rainfall fields at a range of scales of interest (i.e., up to 64×64 km) was investigated. The June 11, 1985, storm was chosen to demonstrate the time evolution of the scaling parameters $\overline{H}$ and $\bar{c}_1$ and their relations to CAPE, since it was the only storm event for which several soundings, coinciding with radar scans appropriate for our analysis, were available (see Table 2 and discussion on data selection in section 3.1). During the period of 0000 to 0600 UTC, 31 radar scans at approximately 10-min time intervals as well as four thermodynamic soundings (at 0000, 0300, 0430, and 0600) from which CAPE was estimated were available. We assumed that between two consecutive soundings, CAPE changed linearly. For each radar scan, $\overline{H}$ and $\bar{c}_1$ were estimated in two ways: (1) directly from the rainfall data and (2) using the measured CAPE values and the developed predictive relationships. This provided a way of evaluating how well physical parameters of the storm environment can predict the rainfall variability at a range of scales of interest. As observed in Figure 11, showing a typical example, the scaling parameters estimated from the radar scans were very close to the predicted values and, often, within their 95% confidence intervals. Also, as expected, positive trends in CAPE estimates usually coincided with positive trends in $\overline{H}$ and with negative trends in $\bar{c}_1$. The same holds true for the opposite case of negative trends in CAPE. The greatest discrepancy between estimated and predicted scaling parameters was observed between 0300 and 0430 UTC. In that period, no information on CAPE was available, and the CAPE values were linearly interpolated between the two measurements at 0300 and 0430 UTC. However, as can be seen from Figure 11, at approximately 0330 UTC the $\overline{H}$ value achieved its maximum and the $\bar{c}_1$ value its minimum. If, according to the correlations obtained, we assumed that the peak CAPE value happened approximately at the same time, the prediction of the scaling parameters would improve noticeably. This assumption is supported by the observational data: the storm was moving into the region in which CAPE=3374 m^2 s^{-2} was estimated from the HET sounding at 0300 UTC. Based on these results, it seems that the relations between CAPE and $\overline{H}$ and between CAPE and $\bar{c}_1$ hold reasonably well during the life cycle of the mesoscale convective system (in this example the tested period corresponds to the mature stage of storm development).

5. Concluding Remarks

The main objective of this paper was to report our findings on the long-standing problem of relating statistical with physical properties of rain. Along these lines we first motivated the need to look for scale invariant statistical descriptions of rainfall since these hold greater promise to relate to the physics of the process than scale dependent descriptions. Based on results of our previous research [*Kumar and Foufoula-Georgiou,* 1993a, b], we decomposed rainfall into "multiscale averages" and "multiscale fluctuations" and posed two main hypotheses: (1) that standardized rainfall fluctuations show scale invariance over the mesoscale (approximately 10^2 to 10^4 km^2) and (2) that the statistical parameterizations of these fluctuations relate to environmental conditions of the prestorm environment. These hypotheses were extensively tested using data from midlatitude mesoscale convective systems observed during the PRE-STORM experiment (May and June 1985) over Oklahoma and Kansas. It was found that ignoring the directionality present in some systems, the standardized rainfall fluctuations can be parameterized by a Gaussian distribution, a scale invariant parameter $\overline{H}$, and a scale dependent parameter $\bar{c}_1$. The parameter $\bar{c}_1$ relates to the variability of the standardized rainfall fluctuations at the specified scale of 8×8 km and the parameter $\overline{H}$ dictates how the variability changes over

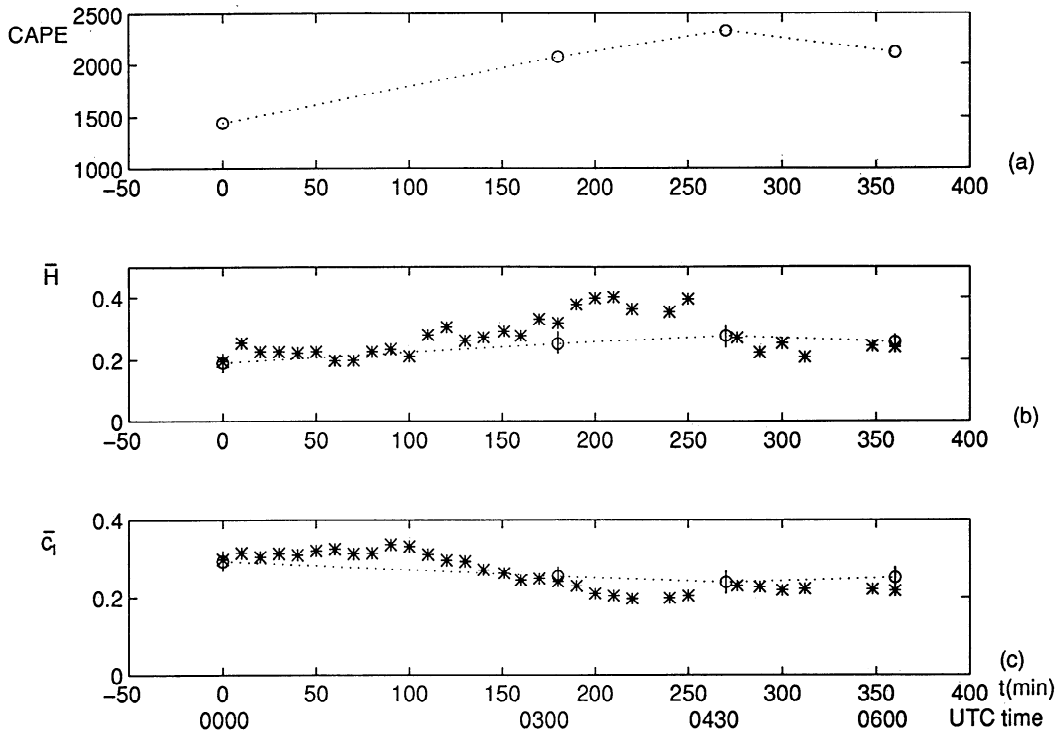

Figure 11. June 11, 1985, storm from 0000 to 0600 UTC. (a) Time evolution of CAPE calculated from representative soundings taken at 0000, 0300, 0430, and 0600 UTC; (b) asterisks represent values of $\overline{H}$ estimated directly from 31 consecutive radar scans and circles connected with dotted lines represent $\overline{H}$ predicted from the regression equation (23) and the corresponding values of CAPE; and (c) same as for Figure 11b but for scaling parameter $\overline{c}_1$. Vertical lines around the circles indicate the 95% confidence intervals.

scales, i.e., $\overline{c}_m = 2^{(m-1)\overline{H}}\,\overline{c}_1$, $m > 1$. If strong directionality is present, then one has at most six parameters $\{H_i, c_{1,i}\}_{i=1,2,3}$, two for each direction (horizontal, vertical, and diagonal).

The parameters $\overline{H}$ and $\overline{c}_1$ were found to depend strongly on the convective instability of the prestorm environment as measured by the convective available potential energy (CAPE). The linear correlations of $\overline{H}$ and $\overline{c}_1$ with CAPE (based on 17 events for which adequate radar rainfall and rawinsonde observations were available) showed that CAPE explains almost 60% of the variability in $\overline{H}$ and $\overline{c}_1$ ($R = 0.82$ and -0.73, respectively). These correlations were interpreted based on physical reasoning.

To our knowledge such quantitative relationships between physical and statistical parameters of rainfall have not been reported previously in the literature. Some previous studies have found strong relationships of maximum parcel energy with maximum rainfall intensities [e.g., *Zawadzki and Ro,* 1978] and a recent study by *Over and Gupta* [1994] has reported strong dependence of a scale invariant parameter (the parameter of the generator of a binomial random cascade model) with large-scale (30×30 km) rainfall averages (interpreted by the authors as indicators of large-scale forcings). Note that in both of the above studies the quantitative relationships between physical and statistical parameters are scale dependent. For example, in the study of *Zawadzki and Ro* [1978], maximal rainfall intensities strongly depend on the resolution of the available rainfall data (sparse data might severely underestimate the true maximum of the storm). Also, in the study of *Over and Gupta* [1994] the "large-scale forcing" has the scale of 30×30 km attached to it, so that using another scale, e.g., 60×60 km averages, will call for different coefficients in the predictive relationship. In our work the predictive relationship between $\overline{H}$ and CAPE (equation (23)) is completely scale independent. The other predictive relationship between $\overline{c}_1$ and CAPE (24) depends on scale (here 8×8 km for the computation of $\overline{c}_1$). If scales other than 8×8 km ($m = 1$) are available, e.g., 16×16 km ($m = 2$), then the predictive relationship becomes

$$\overline{c}_2 = 2^{\overline{H}}\overline{c}_1 = 2^{\overline{H}}[0.3811 - 0.6029(\mathrm{CAPE} \times 10^{-4})].$$

The established predictive relationships between $\overline{H}$ and $\overline{c}_1$ and CAPE are seen as applicable to midlatitude mesoscale convective systems and are envisioned to play an important role in developing subgrid-scale rainfall parameterization models, i.e., models that can resolve the rainfall variability at scales smaller than those resolved by a mesoscale numerical weather prediction model (typically 30 to 60 km). One such model has

recently been developed by the authors and the results will be reported shortly.

Acknowledgments. The authors gratefully acknowledge the help of J. A. Smith and his group at Princeton University in obtaining the PRE-STORM data used in this study. They also gratefully acknowledge the support of NSF (grant EAR-9117866), NOAA (grant NA46GP0486), and NASA (grant NAG 5-2108 and a graduate Global Change Fellowship awarded to the first author). Supercomputer resources were kindly provided by the Minnesota SuperComputer Institute. The authors also acknowledge the helpful comments of an anonymous reviewer.

References

Arad, R. W., Parameter estimation for symmetric stable distribution, *Int. Econ. Rev., 21*(1), 209-220, 1980.

Austin, P. M., and R. A. Houze Jr., Analysis of the structure of precipitation patterns in New England, *J. Appl. Meteorol., 11,* 926-935, 1972.

Barancourt, C., J. D. Creutin, and J. Rivoirard, A method for delineating and estimating rainfall fields, *Water Resour. Res., 28*(4), 1133-1144, 1992.

Blanchard, D. O., Mesoscale convective patterns of the southern High Plains, *Bull. Am. Meteorol. Soc., 71*(7), 994-1005, 1990.

Bluestein, H. B., and M. H. Jain, Formation of mesoscale lines of precipitation: Severe squall lines in Oklahoma during the spring, *J. Atmos. Sci., 42*(16), 1711-1731, 1985.

Cunning, J. B., The Oklahoma-Kansas Preliminary Regional Experiment for STORM-Central, *Bull. Am. Meteorol. Soc., 67*(12), 1478-1486, 1986.

Daubechies, I., *Ten Lectures on Wavelets*, Soc. Industr. Appl. Math., Philadelphia, PA, 1992.

Foufoula-Georgiou, E., and P. Guttorp, Assessment of a class of Neyman-Scott models for temporal rainfall, *J. Geophys. Res., 92,* 9679-9682, 1987.

Foufoula-Georgiou, E., and W. Krajewski, Recent advances in rainfall modeling, estimation, and forecasting, *Rev. Geoph.,*, U.S. Nat. Rep. to Int. Union Geod. and Geoph: 1991-1994, 1125-1137, 1995.

General Meteorological Package (GEMPAK), Version 5.1, Reference manual, Unidata Program Center, UCAR, Boulder, 1992.

Granger, C. W. J., and D. Orr, Infinite variance and research strategy in time series analysis, *J. Am. Stat. Assoc., 67*(338), 275-285, 1972.

Gupta, V. K., and E. Waymire, A statistical analysis of mesoscale rainfall as a random cascade, *J. Appl. Meteorol., 32*(2), 251-267, 1993.

Houze, R. A., B. F. Smull, and P. Dodge, Mesoscale organization of springtime rainstorms in Oklahoma, *Mon. Weather Rev., 118,* 613-654, 1990.

Kumar P., and E. Foufoula-Georgiou, A multicomponent decomposition of spatial rainfall fields, 1. Segregation of large- and small-scale features using wavelet transforms, *Water Resour. Res., 29(8),* 2515-2532, 1993a.

Kumar P., and E. Foufoula-Georgiou, A multicomponent decomposition of spatial rainfall fields, 2. Self-similarity in fluctuations, *Water Resour. Res., 29*(8), 2533-2544, 1993b.

Mallat, S. G., A theory for multiresolution signal decomposition: The wavelet representation, *IEEE Trans. Pattern Anal. Mach. Intel., 11*(7), 674-693, 1989.

Mandelbrot, B., The variation of certain speculative prices, *J. Bus., 36,* 394-419, 1963.

Over, T. M., and V. K. Gupta, Statistical analysis of mesoscale rainfall: Dependence of a random cascade generator on large-scale forcing, *J. Appl. Meteorol., 33*(12), 1526-1542, 1994.

Perica, S., A model for multiscale disaggregation of spatial rainfall based on coupling meteorological and scaling descriptions, Ph.D. thesis, Univ. of Minnesota, Minneapolis, 1995.

Rodriguez-Iturbe, I., V. K. Gupta, and E. Waymire, Scale considerations in the modeling of temporal rainfall, *Water Resour. Res., 20*(11), 1611-1619, 1984.

Tessier, Y., S. Lovejoy, and D. Schertzer, Universal multifractals in rain and clouds: Theory and observations, *J. Appl. Meteorol., 32,* 223-250, 1993.

Waymire, E., V. K. Gupta, and I. Rodriguez-Iturbe, A spectral theory of rainfall intensity at the meso-β scale, *Water Resour. Res., 20*(10), 1453-1465, 1984.

Zawadzki, I. I., and C. U. Ro, Correlations between maximum rate of precipitation and mesoscale parameters, *J. Appl. Meteorol., 17,* 1327-1334, 1978.

Zawadzki, I., E. Torlaschi, and R. Sauvageau, The relationship between mesoscale thermodynamic variables and convective precipitation, *J. Atmos. Sci., 38,* 1535-1540, 1981.

E. Foufoula-Georgiou, Department of Civil Engineering, Saint Anthony Falls Laboratory, University of Minnesota, Mississippi River at 3rd Ave. SE, Minneapolis, MN 55414 (e-mail: efi@mykonos.safhl.umn.edu)

S. Perica, NOAA/NWS/OH3/Hydrologic Research Lab., 1325 East-West Highway, Silver Spring, MD 20910 (e-mail: perica@skipper.ssmc.noaa.gov)

(Received February 13, 1995; revised July 13, 1995; accepted July 14, 1995.)